September 19, 2018

FERMILAB-PUB-94/420-E

Measurement of the B_s Meson Lifetime

F. Abe,[13] M. G. Albrow,[7] D. Amidei,[16] J. Antos,[28] C. Anway-Wiese,[4] G. Apollinari,[26] H. Areti,[7] P. Auchincloss,[25] F. Azfar,[21] P. Azzi,[20] N. Bacchetta,[18] W. Badgett,[16] M. W. Bailey,[18] J. Bao,[34] P. de Barbaro,[25] A. Barbaro-Galtieri,[14] V. E. Barnes,[24] B. A. Barnett,[12] P. Bartalini,[23] G. Bauer,[15] T. Baumann,[9] F. Bedeschi,[23] S. Behrends,[3] S. Belforte,[23] G. Bellettini,[23] J. Bellinger,[33] D. Benjamin,[32] J. Benlloch,[15] J. Bensinger,[3] D. Benton,[21] A. Beretvas,[7] J. P. Berge,[7] S. Bertolucci,[8] A. Bhatti,[26] K. Biery,[11] M. Binkley,[7] F. Bird,[29] D. Bisello,[20] R. E. Blair,[1] C. Blocker,[29] A. Bodek,[25] V. Bolognesi,[23] D. Bortoletto,[24] C. Boswell,[12] T. Boulos,[14] G. Brandenburg,[9] E. Buckley-Geer,[7] H. S. Budd,[25] K. Burkett,[16] G. Busetto,[20] A. Byon-Wagner,[7] K. L. Byrum,[1] J. Cammerata,[12] C. Campagnari,[7] M. Campbell,[16] A. Caner,[7] W. Carithers,[14] D. Carlsmith,[33] A. Castro,[20] Y. Cen,[21] F. Cervelli,[23] J. Chapman,[16] M.-T. Cheng,[28] G. Chiarelli,[8] T. Chikamatsu,[31] S. Cihangir,[7] A. G. Clark,[23] M. Cobal,[23] M. Contreras,[5] J. Conway,[27] J. Cooper,[7] M. Cordelli,[8] D. Crane,[7] J. D. Cunningham,[3] T. Daniels,[15] F. DeJongh,[7] S. Delchamps,[7] S. Dell'Agnello,[23] M. Dell'Orso,[23] L. Demortier,[26] B. Denby,[23] M. Deninno,[2] P. F. Derwent,[16] T. Devlin,[27] M. Dickson,[25] S. Donati,[23] R. B. Drucker,[14] A. Dunn,[16] K. Einsweiler,[14] J. E. Elias,[7] R. Ely,[14] E. Engels, Jr.,[22] S. Eno,[5] D. Errede,[10] S. Errede,[10] Q. Fan,[25] B. Farhat,[15] I. Fiori,[2] B. Flaugher,[7] G. W. Foster,[7] M. Franklin,[9] M. Frautschi,[18] J. Freeman,[7] J. Friedman,[15] A. Fry,[29] T. A. Fuess,[1] Y. Fukui,[13] S. Funaki,[31] G. Gagliardi,[23] S. Galeotti,[23] M. Gallinaro,[20] A. F. Garfinkel,[24] S. Geer,[7] D. W. Gerdes,[16] P. Giannetti,[23] N. Giokaris,[26] P. Giromini,[8] L. Gladney,[21] D. Glenzinski,[12] M. Gold,[18] J. Gonzalez,[21] A. Gordon,[9] A. T. Goshaw,[6] K. Goulianos,[26] H. Grassmann,[6] A. Grewal,[21] G. Grieco,[23] L. Groer,[27] C. Grosso-Pilcher,[5] C. Haber,[14] S. R. Hahn,[7] R. Hamilton,[9] R. Handler,[33] R. M. Hans,[34] K. Hara,[31] B. Harral,[21] R. M. Harris,[7] S. A. Hauger,[6] J. Hauser,[4] C. Hawk,[27] J. Heinrich,[21] D. Cronin-Hennessy,[6]

R. Hollebeek,[21] L. Holloway,[10] A. Hölscher,[11] S. Hong,[16] G. Houk,[21] P. Hu,[22] B. T. Huffman,[22] R. Hughes,[25] P. Hurst,[9] J. Huston,[17] J. Huth,[9] J. Hylen,[7] M. Incagli,[23] J. Incandela,[7] H. Iso,[31] H. Jensen,[7] C. P. Jessop,[9] U. Joshi,[7] R. W. Kadel,[14] E. Kajfasz,[7a] T. Kamon,[30] T. Kaneko,[31] D. A. Kardelis,[10] H. Kasha,[34] Y. Kato,[19] L. Keeble,[30] R. D. Kennedy,[27] R. Kephart,[7] P. Kesten,[14] D. Kestenbaum,[9] R. M. Keup,[10] H. Keutelian,[7] F. Keyvan,[4] D. H. Kim,[7] H. S. Kim,[11] S. B. Kim,[16] S. H. Kim,[31] Y. K. Kim,[14] L. Kirsch,[3] P. Koehn,[25] K. Kondo,[31] J. Konigsberg,[9] S. Kopp,[5] K. Kordas,[11] W. Koska,[7] E. Kovacs,[7a] W. Kowald,[6] M. Krasberg,[16] J. Kroll,[7] M. Kruse,[24] S. E. Kuhlmann,[1] E. Kuns,[27] A. T. Laasanen,[24] S. Lammel,[4] J. I. Lamoureux,[3] T. LeCompte,[10] S. Leone,[23] J. D. Lewis,[7] P. Limon,[7] M. Lindgren,[4] T. M. Liss,[10] N. Lockyer,[21] O. Long,[21] M. Loreti,[20] E. H. Low,[21] J. Lu,[30] D. Lucchesi,[23] C. B. Luchini,[10] P. Lukens,[7] P. Maas,[33] K. Maeshima,[7] A. Maghakian,[26] P. Maksimovic,[15] M. Mangano,[23] J. Mansour,[17] M. Mariotti,[23] J. P. Marriner,[7] A. Martin,[10] J. A. J. Matthews,[18] R. Mattingly,[15] P. McIntyre,[30] P. Melese,[26] A. Menzione,[23] E. Meschi,[23] G. Michail,[9] S. Mikamo,[13] M. Miller,[5] R. Miller,[17] T. Mimashi,[31] S. Miscetti,[8] M. Mishina,[13] H. Mitsushio,[31] S. Miyashita,[31] Y. Morita,[13] S. Moulding,[26] J. Mueller,[27] A. Mukherjee,[7] T. Muller,[4] P. Musgrave,[11] L. F. Nakae,[29] I. Nakano,[31] C. Nelson,[7] D. Neuberger,[4] C. Newman-Holmes,[7] L. Nodulman,[1] S. Ogawa,[31] S. H. Oh,[6] K. E. Ohl,[34] R. Oishi,[31] T. Okusawa,[19] C. Pagliarone,[23] R. Paoletti,[23] V. Papadimitriou,[7] S. Park,[7] J. Patrick,[7] G. Pauletta,[23] M. Paulini,[14] L. Pescara,[20] M. D. Peters,[14] T. J. Phillips,[6] G. Piacentino,[2] M. Pillai,[25] R. Plunkett,[7] L. Pondrom,[33] N. Produit,[14] J. Proudfoot,[1] F. Ptohos,[9] G. Punzi,[23] K. Ragan,[11] F. Rimondi,[2] L. Ristori,[23] M. Roach-Bellino,[32] W. J. Robertson,[6] T. Rodrigo,[7] J. Romano,[5] L. Rosenson,[15] W. K. Sakumoto,[25] D. Saltzberg,[5] A. Sansoni,[8] V. Scarpine,[30] A. Schindler,[14] P. Schlabach,[9] E. E. Schmidt,[7] M. P. Schmidt,[34] O. Schneider,[14] G. F. Sciacca,[23] A. Scribano,[23] S. Segler,[7] S. Seidel,[18] Y. Seiya,[31] G. Sganos,[11] A. Sgolacchia,[2] M. Shapiro,[14] N. M. Shaw,[24] Q. Shen,[24] P. F. Shepard,[22] M. Shimojima,[31] M. Shochet,[5] J. Siegrist,[29] A. Sill,[7a] P. Sinervo,[11] P. Singh,[22] J. Skarha,[12] K. Sliwa,[32] D. A. Smith,[23] F. D. Snider,[12] L. Song,[7] T. Song,[16] J. Spalding,[7] L. Spiegel,[7] P. Sphicas,[15] A. Spies,[12] L. Stanco,[20] J. Steele,[33] A. Stefanini,[23] K. Strahl,[11] J. Strait,[7] D. Stuart,[7] G. Sullivan,[5]

K. Sumorok,[15] R. L. Swartz, Jr.,[10] T. Takahashi,[19] K. Takikawa,[31] F. Tartarelli,[23] W. Taylor,[11] Y. Teramoto,[19] S. Tether,[15] D. Theriot,[7] J. Thomas,[29] T. L. Thomas,[18] R. Thun,[16] M. Timko,[32] P. Tipton,[25] A. Titov,[26] S. Tkaczyk,[7] K. Tollefson,[25] A. Tollestrup,[7] J. Tonnison,[24] J. F. de Troconiz,[9] J. Tseng,[12] M. Turcotte,[29] N. Turini,[2] N. Uemura,[31] F. Ukegawa,[21] G. Unal,[21] S. van den Brink,[22] S. Vejcik, III,[16] R. Vidal,[7] M. Vondracek,[10] R. G. Wagner,[1] R. L. Wagner,[7] N. Wainer,[7] R. C. Walker,[25] G. Wang,[23] J. Wang,[5] M. J. Wang,[28] Q. F. Wang,[26] A. Warburton,[11] G. Watts,[25] T. Watts,[27] R. Webb,[30] C. Wendt,[33] H. Wenzel,[14] W. C. Wester, III,[14] T. Westhusing,[10] A. B. Wicklund,[1] E. Wicklund,[7] R. Wilkinson,[21] H. H. Williams,[21] P. Wilson,[5] B. L. Winer,[25] J. Wolinski,[30] D. Y. Wu,[16] X. Wu,[23] J. Wyss,[20] A. Yagil,[7] W. Yao,[14] K. Yasuoka,[31] Y. Ye,[11] G. P. Yeh,[7] P. Yeh,[28] M. Yin,[6] J. Yoh,[7] T. Yoshida,[19] D. Yovanovitch,[7] I. Yu,[34] J. C. Yun,[7] A. Zanetti,[23] F. Zetti,[23] L. Zhang,[33] S. Zhang,[15] W. Zhang,[21] and S. Zucchelli[2]

(CDF Collaboration)

[1] *Argonne National Laboratory, Argonne, Illinois 60439*

[2] *Istituto Nazionale di Fisica Nucleare, University of Bologna, I-40126 Bologna, Italy*

[3] *Brandeis University, Waltham, Massachusetts 02254*

[4] *University of California at Los Angeles, Los Angeles, California 90024*

[5] *University of Chicago, Chicago, Illinois 60637*

[6] *Duke University, Durham, North Carolina 27708*

[7] *Fermi National Accelerator Laboratory, Batavia, Illinois 60510*

[8] *Laboratori Nazionali di Frascati, Istituto Nazionale di Fisica Nucleare, I-00044 Frascati, Italy*

[9] *Harvard University, Cambridge, Massachusetts 02138*

[10] *University of Illinois, Urbana, Illinois 61801*

[11] *Institute of Particle Physics, McGill University, Montreal H3A 2T8, and University of Toronto, Toronto M5S 1A7, Canada*

[12] *The Johns Hopkins University, Baltimore, Maryland 21218*

[13] *National Laboratory for High Energy Physics (KEK), Tsukuba, Ibaraki 305, Japan*

[14] *Lawrence Berkeley Laboratory, Berkeley, California 94720*

[15] *Massachusetts Institute of Technology, Cambridge, Massachusetts 02139*

[16] *University of Michigan, Ann Arbor, Michigan 48109*

[17] *Michigan State University, East Lansing, Michigan 48824*

[18] *University of New Mexico, Albuquerque, New Mexico 87131*

[19] *Osaka City University, Osaka 588, Japan*

[20] *Universita di Padova, Instituto Nazionale di Fisica Nucleare, Sezione di Padova, I-35131 Padova, Italy*

[21] *University of Pennsylvania, Philadelphia, Pennsylvania 19104*

[22] *University of Pittsburgh, Pittsburgh, Pennsylvania 15260*

[23] *Istituto Nazionale di Fisica Nucleare, University and Scuola Normale Superiore of Pisa, I-56100 Pisa, Italy*

[24] *Purdue University, West Lafayette, Indiana 47907*

[25] *University of Rochester, Rochester, New York 14627*

[26] *Rockefeller University, New York, New York 10021*

[27] *Rutgers University, Piscataway, New Jersey 08854*

[28] *Academia Sinica, Taiwan 11529, Republic of China*

[29] *Superconducting Super Collider Laboratory, Dallas, Texas 75237*

[30] *Texas A&M University, College Station, Texas 77843*

[31] *University of Tsukuba, Tsukuba, Ibaraki 305, Japan*

[32] *Tufts University, Medford, Massachusetts 02155*

[33] *University of Wisconsin, Madison, Wisconsin 53706*

[34] *Yale University, New Haven, Connecticut 06511*

The lifetime of the B_s meson is measured using the semileptonic decay $B_s \to D_s^- \ell^+ \nu X$. The data sample consists of 19.3 pb^{-1} of $p\bar{p}$ collisions at $\sqrt{s} = 1.8$ TeV collected by the CDF detector at the Fermilab Tevatron collider during 1992-1993. There are 76 ± 8 $\ell^+ D_s^-$ signal events where the D_s is identified via the decay $D_s^- \to$

$\phi\pi^-$, $\phi \to K^+K^-$. Using these events, the B_s meson lifetime is determined to be $\tau_s = 1.42\ ^{+0.27}_{-0.23}$ (stat) $\pm$ 0.11 (syst) ps. A measurement of the B_s lifetime in a low statistics sample of exclusive $B_s \to J/\psi\phi$ decays is also presented in this paper.

PACS numbers: 13.25.Hw, 14.40.Nd

The lifetime differences between the bottom hadrons can probe the B-decay mechanisms which are beyond the simple quark spectator model. In the case of charm mesons, such differences have been observed to be quite large ($\tau(D^+)/\tau(D^0) \sim 2.5$). Among bottom hadrons, the lifetime differences are expected to be smaller due to the heavier bottom quark mass. Phenomenological models predict a 5-10% difference between the B_u and B_d meson lifetimes and very similar B_d and B_s lifetimes [1]. This is consistent with the previous measurements of $B_{u,d}$ meson lifetime [2], as well as recent B_s lifetime measurements from LEP [3]. It has also been suggested by recent theory calculations [4] that the lifetime between the two CP eigenstates produced by mixing of the B_s and $\overline{B}_s$ may differ by as much as 15%. Such an effect may manifest itself as a difference in lifetimes between the B_s semileptonic decay, which is almost an equal mixture of the two CP states, and the decay $B_s \to J/\psi\phi$, which is expected to be dominated by the CP even state. In this letter, we first present the measurement of B_s lifetime using the semileptonic decay [5] $B_s \to D_s^- \ell^+ \nu X$, where the D_s^- is identified via $D_s^- \to \phi\pi^-,\ \phi \to K^+K^-$. We then describe briefly a result using the exclusive decay $B_s \to J/\psi\phi$, where $J/\psi \to \mu^+\mu^-,\ \phi \to K^+K^-$. The data sample for this paper consists of 19.3 pb^{-1} of $p\overline{p}$ collisions at $\sqrt{s}$=1.8 TeV collected by the CDF detector during the 1992-1993 run.

The CDF detector is described in detail elsewhere [6]. We describe here only the detector features most relevant to this analysis. Two devices inside the 1.4 T solenoid are used for the tracking of charged particles: the silicon vertex detector (SVX) and the central tracking chamber (CTC). The SVX consists of four layers of silicon microstrip detectors located at radii between 3.0 and 7.9 cm from the interaction point and provides spatial measurements in the r-φ plane [7] with a resolution of 13 μm, giving a track impact parameter resolution of about $(13+40/p_T)$ μm [8], where p_T is the transverse momentum of the track in GeV/c. The transverse profile of the beam is circular and has an RMS of $\sim$ 35 μm, while the longitudinal beam size is $\sim$ 30 cm. The CTC is a cylindrical drift chamber containing 84 layers grouped into 8 alternating superlayers of axial and stereo wires. It covers the pseudorapidity interval $|\eta| < 1.1$, where $\eta = -\ln[\tan(\theta/2)]$. The p_T resolution of the CTC combined with the SVX

is $\delta(p_T)/p_T = ((0.0066)^2 + (0.0009 p_T)^2)^{1/2}$. Outside the solenoid are electromagnetic (CEM) and hadronic (CHA) calorimeters ($|\eta| < 1.1$) that employ a projective tower geometry. A layer of proportional wire chambers (CES) is located near shower maximum in the CEM and provides a measurement of electromagnetic shower profiles in both the φ and z directions. Two different muon subsystems in the central region are used, the central muon chambers (CMU) and the central upgrade muon chambers (CMP), with total coverage of 80% for $|\eta| \leq 0.6$. The CMP chambers are located behind 8 interaction lengths of material.

Events containing semileptonic B_s decays were collected using inclusive electron and muon triggers. The E_T threshold for the principal single electron trigger was 9 GeV, where $E_T \equiv E \sin(\theta)$ and E is the electromagnetic energy measured in the calorimeter. The single muon trigger required a $p_T > 7.5$ GeV/c track in the CTC with matched track segments in both the CMU and CMP systems.

Offline identification of an electron [9] involved measurements from both the calorimeters and the CTC. Photon conversion electrons were removed by searching for an oppositely charged track which had a small opening angle with a primary electron candidate.

A muon candidate was required to be detected by both the CMU and CMP chambers to reduce background due to hadrons that do not interact in the calorimeter. Good position matching [10] was required between track segments in the muon chambers and an extrapolated CTC track.

The $D_s^- \to \phi\pi^-$ reconstruction started with a search for ϕ candidates. We first defined a search cone around the lepton candidate with a radius $\Delta R = \sqrt{\Delta\eta^2 + \Delta\varphi^2}$ of 0.8. Any two oppositely charged tracks with $p_T > 1$ GeV/c within that cone were assigned kaon masses and combined to form a ϕ candidate. No kaon identification was used in the ϕ selection. Each ϕ candidate was required to have $p_T(\phi) > 2.0$ GeV/c and a mass within ± 8 MeV/c^2 of the world average ϕ mass [11]. The ϕ candidate was then combined with another track of $p_T > 0.8$ GeV/c inside the cone which had the opposite charge of the lepton (the 'right-sign' combination). This third track was assigned the pion mass. To ensure a good decay vertex

measurement, track quality cuts were imposed on the lepton and at least two of the three track candidates forming the D_s candidate. The K^+, K^-, and π^- tracks were then refit with a common vertex constraint. The confidence level of that fit was required to be greater than 1%. Since the ϕ has spin 1 and both the D_s^- and π^- are spin 0, the helicity angle Ψ, which is the angle between the K^+ and D_s^- directions in the ϕ rest frame exhibits a distribution $dN/d(\cos\Psi) \sim \cos^2\Psi$. A cut $|\cos\Psi| > 0.4$ was therefore applied to suppress the combinatorial background, which we found to be a flat in $\cos\Psi$ distribution. The mass of the ℓD_s system was required to be between 3.0 and 5.7 GeV/c^2 in order to be consistent with coming from a B_s decay. We also applied an isolation cut $E_T^{\rm iso}/p_T(\phi\pi^-) < 1.2$ on the D_s^- candidate, where $E_T^{\rm iso}$ is a sum of transverse energy within a cone of radius 0.4 in η-φ space around the lepton candidate, excluding the lepton energy. This cut eliminated many of the fake D_s^- combinations from high track multiplicity jets. Furthermore, we required that the apparent D_s^- decay vertex (V_{D_s}) be positively displaced from the primary vertex along the direction of the $\ell^+ D_s^-$ momentum. Figure 1a shows the $\phi\pi^-$ invariant mass distribution for the 'right-sign' lepton-D_s combinations. A D_s signal with mean of 1.967 GeV/c^2 and width of 5.4 MeV/c^2 is observed. Evidence of the Cabibbo suppressed $D^- \to \phi\pi^-$ decay is also present. No enhancement is seen in the corresponding distribution for the 'wrong-sign' combinations (Figure 1b). We select a signal sample using a D_s^- mass window of 1.953 to 1.981 GeV/c^2. A total of 139 events are found with a background fraction $f_{bg} = 0.45 \pm 0.01$. The number of $\ell^+ D_s^-$ events above background in the sample is 76 ± 8.

There are two possible sources of non-strange B meson decays which can lead to right-sign $\ell^+ D_s^-$ combinations. The first one is a four body decay $B_{u,d} \to D_s^- \mathbf{K} \ell^+ \nu$, where $\mathbf{K}$ denotes any type of strange meson. Because of the low probability of producing $s\overline{s}$ pairs and the limited phase space, this process is suppressed and has not been observed experimentally. The recent ARGUS limit (90% CL) is $\mathrm{BR}(B_{u,d} \to D_s^- \mathbf{K} \ell^+ \nu) < 1.2\%$ [12]. Also, a theoretical analysis based on the 'resonance model' yields $\mathrm{BR}(B_{u,d} \to D_s^- \mathbf{K} \ell^+ \nu) \leq 0.025 \times \mathrm{BR}(B_d \to \ell^+ \nu X)$ [13]. Using the latter result and our estimated efficiency, we expect less than 2.6% of our $\ell^+ D_s^-$ combinations from this source. The second process is $\overline{B}_{u,d} \to D_s^- D X, D \to \ell^+ \nu X$,

where D is any charmed meson. This decay produces softer and less isolated leptons than that from B_s semileptonic decay and therefore the acceptance for this source relative to the signal is quite small ($\sim 2.6\%$). Using the BR($B \to D_s X$) [14,15] and the semileptonic branching ratios of D^0 and D^+ [11], we estimate the fraction of this type of background is less than 3%. In addition, we also considered the background from $c\overline{c}$ production where a $D_s^- D$ pair is produced. Monte Carlo predicts the background fraction from this type of source to be $< 7\%$. In summary, the contribution of all above physics backgrounds is quite small compared to the combinatorial background. We will consider them as a source of systematic uncertainty for the B_s lifetime measurement.

The secondary vertex where the B_s decays to a lepton and a D_s^- (referred to as V_{B_s}) is obtained by intersecting the trajectory of the lepton track with the flight path of the D_s^- candidate. The transverse decay length L is defined as the displacement in the transverse plane of V_{B_s} from the primary vertex projected onto the direction of the $p_T(\ell D_s)$. This is our best estimator of the B_s direction. The effect of the unknown B_s relativistic boost can be partially removed event-by-event with the factor $p_T(\ell D_s)/M(B_s)$ (where $M(B_s) = 5.37$ GeV/c^2 [16]) and leads to a corrected decay length

$$\xi = \frac{L \cdot M(B_s)}{p_T(\ell D_s)}, \tag{1}$$

which is referred to as the 'proper decay length'. A residual correction between $p_T(\ell D_s)$ and $p_T(B_s)$ is done statistically by convoluting a Monte Carlo distribution of the p_T correction factor K$= p_T(\ell D_s)/p_T(B_s)$ with an exponential decay distribution in the lifetime fit. The K distribution has an average value of 0.86 and an RMS of 0.11 and is approximately constant as a function of $p_T(\ell D_s)$. To model the proper decay length distribution of the background events contained in the signal sample, we define a background sample which consists of the right-sign events from the D_s^- sidebands (1.885-1.945 and 1.990-2.050 GeV/c^2) and the wrong-sign events from the interval 1.885-2.050 GeV/c^2.

The proper decay length distribution (Figure 2) is fit using an unbinned maximum log-likelihood method. Both the B_s lifetime and the background shape are determined in a

simultaneous fit using the signal and background samples. Thus the likelihood function $\mathcal{L}$ is a combination of two parts:

$$\mathcal{L} = \prod_{i}^{N_S}[(1 - f_{bg})\mathcal{F}^i_{Sig} + f_{bg}\mathcal{F}^i_{bg}] \cdot \prod_{j}^{N_B}\mathcal{F}^j_{bg}, \tag{2}$$

where N_S and N_B are the number of events in the signal and background samples. The signal probability function $\mathcal{F}_{Sig}$ consists of a normalized decay exponential function (defined for only positive decay lengths and symbolized by $\mathcal{E}_+$) convoluted with the K distribution and a Gaussian resolution function $\mathcal{G}$:

$$\mathcal{F}^i_{Sig}(c\tau, \mathbf{s}) = \mathcal{E}_+(-Kx, c\tau) \otimes K^{dist} \otimes \mathcal{G}(\xi^i - x, \mathbf{s}\sigma^i), \tag{3}$$

where ξ^i is the measured proper decay length with uncertainty σ^i (typically 100μm) and x is the true proper decay length. The scale factor $\mathbf{s}$ accounts for the underestimation of the decay length error. The background is parameterized by a Gaussian centered at zero, symmetrical positive and negative exponential tails, and a positive decay exponential to characterize the heavy flavor decay in the background sample.

The best fit values of $c\tau$ and s are found to be $426\ ^{+\ 80}_{-\ 68}$ μm and $1.4\ \pm 0.1$ respectively. Figure 2a shows the proper decay length distribution of the signal sample with the result of the fit superimposed. The same distribution of the background samples is shown in Figure 2b. As a consistency check, we also fit the D_s lifetime from the proper decay length measured from the tertiary vertex V_{D_s} to the secondary vertex V_{B_s}. The result is $c\tau(D_s) = 135\ ^{+\ 40}_{-\ 30}$ μm, which is consistent with the world average value [11].

Table I lists all sources of systematic uncertainty considered in this analysis. Major contributions come from the source of the background shape, the non-B_s production, and the resolution function. To model the contribution to the signal from the combinatorial backgrounds, we combined the events from three different sideband regions. There may be some bias in choosing the correct mixture. We find a $\pm$ 4% variation in the lifetime when using each sideband region individually. The dominant source of systematics from non-B_s production was found to be $\overline{B}_{u,d} \to D_s^- DX$ decays. This mode was studied using Monte

Carlo simulations and the contribution to the systematic uncertainty in the lifetime was found to $\pm$ 4%. The effect of the decay length resolution was studied by varying the scale factor and using an alternative resolution function consisting of two Gaussians, giving a 3% systematic uncertainty.

Quoting the statistical and systematic uncertainties separately, we measure the B_s lifetime using semileptonic decays to be

$$\tau_{B_s} = 1.42\ ^{+0.27}_{-0.23}\ (\text{stat})\ \ ^{+0.11}_{-0.11}\ (\text{syst})\ \text{ps}.$$

This result is consistent with the previous world average of $1.34\ ^{+0.32}_{-0.27}$ ps [11].

For the exclusive mode measurement, we use the decay chain $B_s \to J/\psi\phi$, $J/\psi \to \mu^+\mu^-$, $\phi \to K^+K^-$. The data sample and reconstruction techniques used for this decay channel are similar to those described in detail elsewhere [17]. Briefly, the invariant mass of two oppositely charged muon candidates is calculated after the tracks are constrained to originate from a common vertex. J/ψ candidates are selected by requiring the difference between the dimuon mass and the world average J/ψ mass [11] to be $< 3\sigma$, where σ is the mass uncertainty calculated for each dimuon candidate. The ϕ meson selections are the same as reference [17] but with $p_T(\phi) > 3.0$ (rather than 2 GeV/c) to further reduce the background. To reconstruct B_s meson candidates, the 4 daughter tracks are constrained to originate from a common vertex and the dimuon mass is simultaneously constrained to the world average J/ψ mass. We require the χ^2 probability for this combined fit to be $> 2\%$. In addition, at least one of the μ candidates and at least one of the other tracks must be well measured in the SVX.

Using the measured $p_T(B_s)$, the proper decay length is calculated and the lifetime of the B_s meson is determined by performing a simultaneous unbinned log-likelihood fit to the entire mass and proper decay length spectra. The mass distribution is fit to a Gaussian and a flat background. We model the proper decay length distribution of the background with a Gaussian centered at zero and positive and negative exponential functions. The signal is described by an exponential decay function convoluted with a Gaussian. This fit determines

the mass and lifetime of the B_s, the signal fraction, and background shape simultaneously. The proper decay length distribution is shown in Figure 3, where we have displayed events within ± 21 MeV/c^2 of the B_s mass peak. The fit returns $7.9\ ^{+3.6}_{-1.6}$ signal events and a B_s lifetime of $c\tau_{B_s} = 520\ ^{+330}_{-210}\ \mu$m.

We estimate a total systematic error of $\pm 20\mu$m, the dominant contributions arising from the uncertainty in the parametrization of the background shape and our understanding of the resolution function. The B_s lifetime using fully reconstructed $B_s \to J/\psi\phi$ decays is measured to be:

$$\tau_{B_s} = 1.74\ ^{+1.08}_{-0.69}\ \text{(stat.)}\ \pm 0.07\ \text{(syst.)}\ \text{ps}.$$

In conclusion, the B_s lifetime has been measured in both the semileptonic and exclusive decay channels. At present, the two measurements are consistent with each other within their quoted uncertainties and are consistent with the results of the B_u and B_d lifetimes previously measured by CDF.

We anticipate a more significant result in both modes after the ongoing collider run.

We thank the Fermilab staff and the technical staffs of the participating institutions for their vital contributions. This work was supported by the U.S. Department of Energy and National Science Foundation; the Italian Istituto Nazionale di Fisica Nucleare; the Ministry of Education, Science and Culture of Japan; the Natural Sciences and Engineering Research Council of Canada; the National Science Council of the Republic of China; the A. P. Sloan Foundation; and the Alexander von Humboldt-Stiftung.

TABLES

TABLE I. Semileptonic mode systematic uncertainties.

Systematic Source	Uncertainty
Background shape	4%
Non-B_s source	4%
Resolution function	3%
Boost correction	2%
Decay length cut	2%
Fitting method	1%
Misalignment	2%
Total	7%

REFERENCES

[1] M. B. Voloshin and M. A. Shifman, Sov. Phys. JETP **64**, 698 (1986).

[2] F. Abe *et al.,* Phys. Rev. Lett. **72** 3456 (1994); S. Wagner *et al.,* Phys. Rev. Lett. **64** 1095 (1990); P. Abreu *et al.,* Z. Phys. **C 57** 181 (1993); D. Buskulic *et al.,* Phys. Lett. **B 297** 449 (1992); D. Buskulic *et al.,* Phys. Lett. **B 307** 194 (1993); D. Buskulic *et al.,* Phys. Lett. **B 314** 459 (1993); P. D. Acton *et al.,* Phys. Lett. **B 307** 247 (1993).

[3] P. D. Acton *et al.*, Phys. Lett. **B 312** 501 (1993); P. Abreu *et al.,* Z. Phys. **C 61** 407 (1994); D. Buskulic *et al.,* Phys. Lett. **B 322** 275 (1994).

[4] I. I. Bigi *et al.*, CERN-TH.7132/94; R. Aleksan *et al.*, Phys. Lett. **B 316** (1993) 567.

[5] References to a specific charge state imply the charge-conjugate state as well.

[6] F. Abe *et al.,* Nucl. Instr. and Meth. **A271** (1988) 387, and references therein.

[7] In CDF, φ is the azimuthal angle, θ is the polar angle measured from the proton direction, and r is the radius from the beam axis (z-axis).

[8] D. Amidei *et al.,* Nucl. Instrum. Methods Phys. Res. , Sect. **A 350**, 73 (1994)

[9] F. Abe *et al.,* Phys. Rev. Lett. **71** 500 (1993).

[10] F. Abe *et al.,* Phys. Rev. Lett. **71** 3421 (1993).

[11] Particle Data Group, M. Aguilar-Benitez *et al.*, Phys. Rev. D **50**, (1994).

[12] H. Albrecht *et al.,* Z. Phys. **C 60** (1993) 11.

[13] E. Golowich *et al.,* Z. Phys. **C 48** (1990) 89.

[14] D. Bortoletto *et al.,* Phys. Rev. Lett. **64** (1990) 2117.

[15] H. Albrecht *et al.,* Z. Phys. **C 54** (1992) 1.

[16] Y. Cen, Ph.D. thesis, University of Pennsylvania, 1994 (unpublished).

[17] F. Abe *et al.*, Phys. Rev. Lett. **71** 1685 (1993).

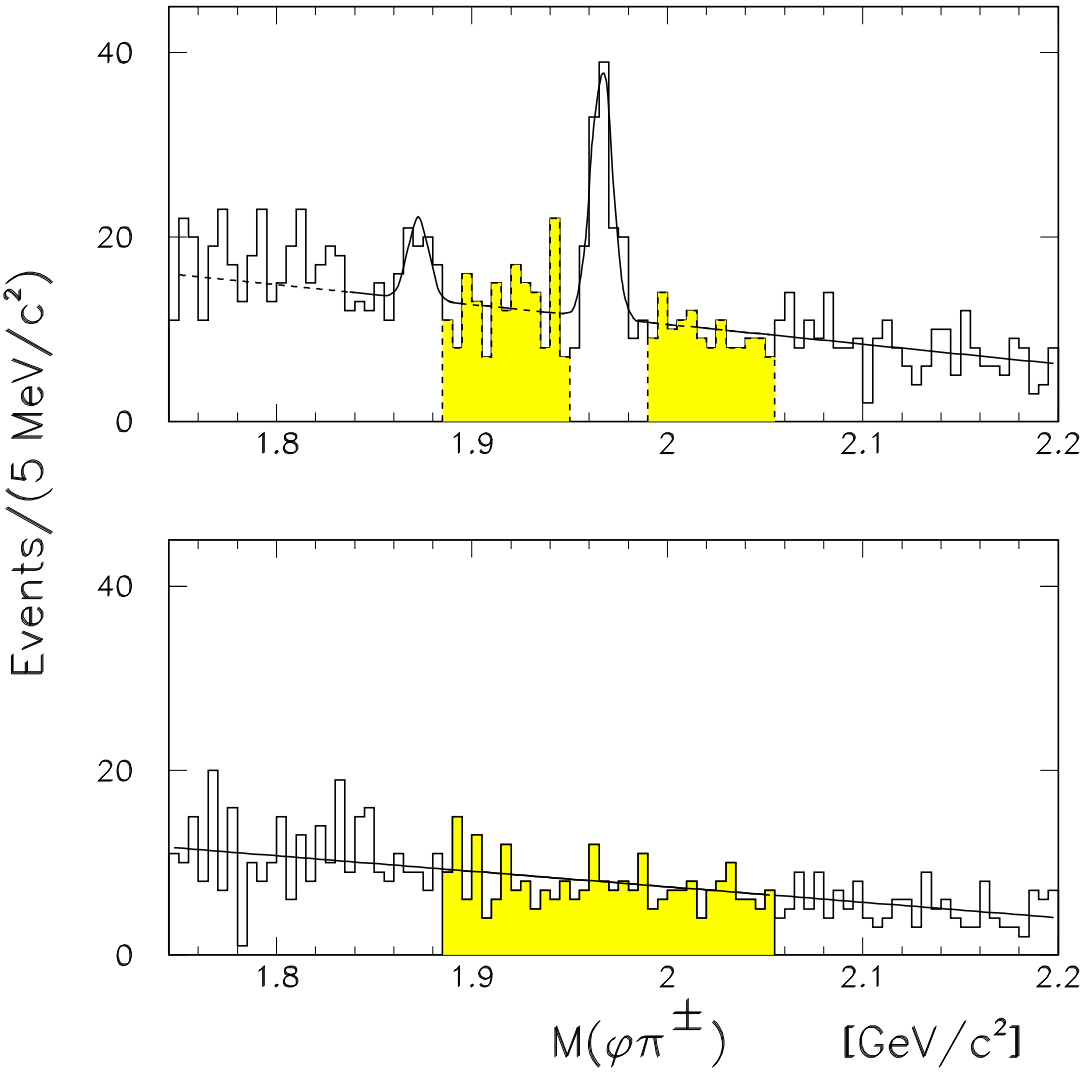

FIG. 1.

The mass distribution of $\phi\pi^-$ for (a) 'right-sign' combination ($\phi\pi^-\ell^+$); (b) 'wrong-sign' combination ($\phi\pi^-\ell^-$).The shaded regions are used for the background sample.

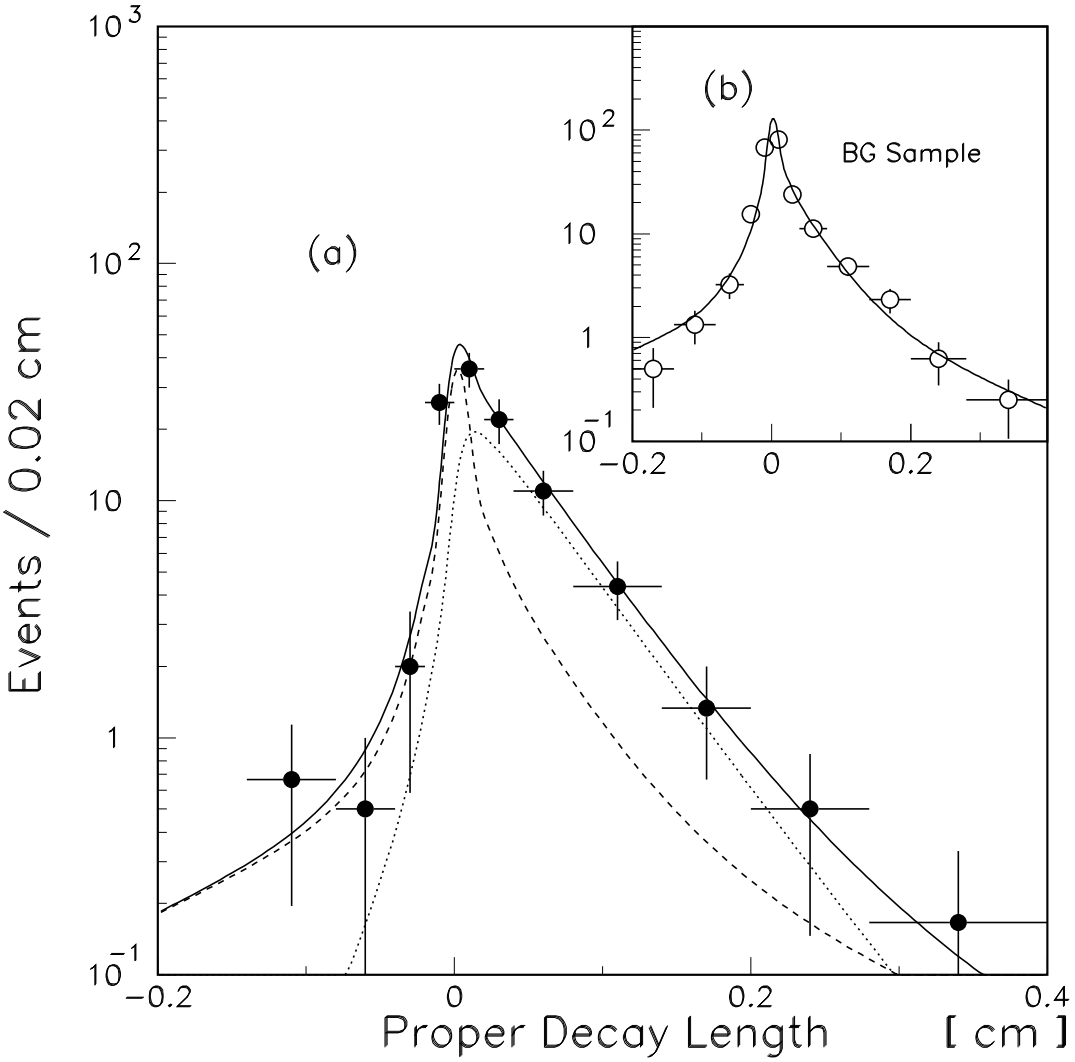

FIG. 2.

(a) Proper decay length distribution for the $\ell^+ D_s^-$ signal sample with a curve (solid) from unbinned log-likelihood fitting of signal and background. The dashed line represents the contribution from the combinatorial background. The dotted one represents the signal contribution. (b) The proper decay length distribution for the background sample with a curve representing the background lifetime contribution.

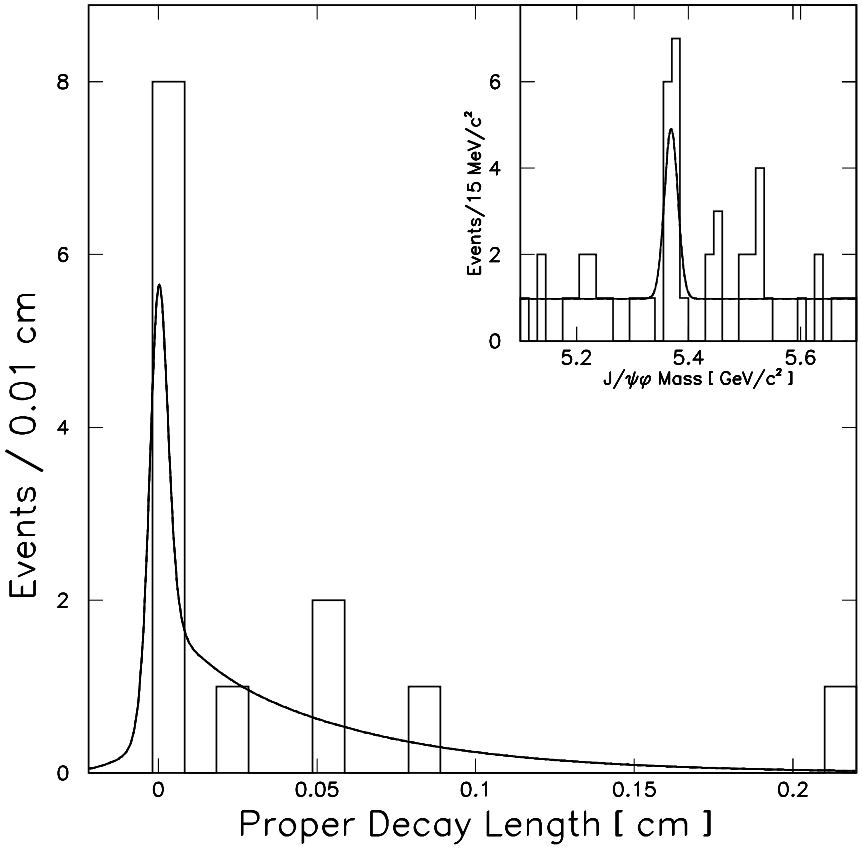

FIG. 3.

B_s lifetime measurement using the $J/\psi\phi$ exclusive mode. Inset figure is the mass distribution. The solid curves show the fit results.